© 2020. Published by The Company of Biologists Ltd | Journal of Experimental Biology (2020) 223, jeb204438. doi:10.1242/jeb.204438

RESEARCH ARTICLE

A cerebellum-like circuit in the lateral line system of fish cancels mechanosensory input associated with its own movements

Krista E. Perks[1,2,3,*], Anna Krotinger[2,3] and David Bodznick[2,3]

ABSTRACT

An animal's own movement exerts a profound impact on sensory input to its nervous system. Peripheral sensory receptors do not distinguish externally generated stimuli from stimuli generated by an animal's own behavior (reafference) – although the animal often must. One way that nervous systems can solve this problem is to provide movement-related signals (copies of motor commands and sensory feedback) to sensory systems, which can then be used to generate predictions that oppose or cancel out sensory responses to reafference. Here, we studied the use of movement-related signals to generate sensory predictions in the lateral line medial octavolateralis nucleus (MON) of the little skate. In the MON, mechanoreceptive afferents synapse on output neurons that also receive movement-related signals from central sources, via a granule cell parallel fiber system. This parallel fiber system organization is characteristic of a set of so-called cerebellum-like structures. Cerebellum-like structures have been shown to support predictive cancellation of reafference in the electrosensory systems of fish and the auditory system of mice. Here, we provide evidence that the parallel fiber system in the MON can generate predictions that are negative images of (and therefore cancel) sensory input associated with respiratory and fin movements. The MON, found in most aquatic vertebrates, is probably one of the most primitive cerebellum-like structures and a starting point for cerebellar evolution. The results of this study contribute to a growing body of work that uses an evolutionary perspective on the vertebrate cerebellum to understand its functional diversity in animal behavior.

KEY WORDS: Cerebellum-like, Mechanosensory lateral line, Predictive cancellation, Reafference, Elasmobranch, Sensory system

INTRODUCTION

Sensory systems face the particular challenge that an animal's own motor acts generate sensory stimuli (called reafference) that can obscure and distract from externally generated signals of interest. In some cases, inhibitory motor-related signals are sufficient to gate out brief, stereotyped reafference from the system (Bell and Grant, 1989; Kim et al., 2017, 2015; Poulet and Hedwig, 2003). However, animals and environments are varied and complex, and associations between signals and behavior appear, change and disappear over time. Studies of the electrosensory systems of three phylogenetically distinct taxa of fish have provided unique insights into the general issue of how responses to expected stimuli such as reafference are eliminated by predictions based on central signals associated with the animal's own movements and behavior (Bastian, 1995; Bell et al., 1981; Montgomery and Bodznick, 1994; Requarth and Sawtell, 2014). The first stage of processing in this and several other sensory systems occurs in hindbrain structures that share numerous similarities with the cerebellum in terms of their evolution, development, patterns of gene expression and circuitry and are therefore termed 'cerebellum-like' (Bell et al., 1997a, 2008; Bell, 2002; Suriano and Bodznick, 2018).

A distinguishing feature of a class of cerebellum-like sensory structures is the integration of direct input from peripheral sensory receptors with a diverse array of sensory and motor signals conveyed by a granule cell–parallel fiber system. *In vitro* and *in vivo* electrophysiological studies and computational modeling of cerebellum-like electrosensory structures all point to a common functional logic for this cerebellum-like organization. In electrosensory and auditory systems, the parallel fiber system continually generates and updates sensory predictions based on associations between central signals and peripheral sensory inputs (Bastian, 1995; Bell et al., 1981; Montgomery and Bodznick, 1994; Singla et al., 2017). These predictions are generated based on anti-Hebbian synaptic plasticity rules, sometimes termed decorrelation learning rules, and are observed in the spiking and subthreshold membrane potential of single principal neurons as a response to parallel fiber input that is negatively correlated with the responses driven by expected sensory input (Bastian, 1996; Bell et al., 1993, 1997b; Bodznick et al., 1999; Harvey-Girard et al., 2010; Montgomery and Bodznick, 1994; Nelson and Paulin, 1995; Roberts and Bell, 2000). This negative image or cancellation signal, when subtracted from the neural response, therefore eliminates responses to expected sensory input while maintaining sensitivity to unexpected stimuli (Enikolopov et al., 2018). Cancellation of reafference by the electrosensory cerebellum-like circuit is therefore an active memory-based process.

Although they have evolved independently, the electrosensory systems of elasmobranch, mormyriform and gymnotiform fishes share important similarities in the structure and function of their cerebellum-like electrosensory structures at the first stage of sensory processing (Bell, 2002; Bullock et al., 1983; Finger et al., 1986; Montgomery et al., 2012). These observations suggest that the evolutionarily convergent cerebellum-like circuitry in each case provides a mechanism for generating predictions based on the animal's own behavior that eliminate responses to expected sensory input. Consistent with this hypothesis, a recent study of the dorsal cochlear nucleus in mice demonstrates that the cerebellum-like circuit at this first central stage of auditory processing is associated with the elimination of reafference from the output of the dorsal cochlear nucleus (Oertel and Young, 2004; Singla et al., 2017).

The medial octavolateral nucleus (MON) found in most aquatic vertebrates may be the most primitive cerebellum-like structure. The

[1]Neurosciences Department and Zuckermann Institute, Columbia University, New York, NY 10027, USA. [2]Neuroscience & Behavior Program and Department of Biology, Wesleyan University, Middletown, CT 06459, USA. [3]Marine Biological Laboratory, Woods Hole, MA 02543, USA.

*Author for correspondence (kep2142@columbia.edu)

K.E.P., 0000-0003-3804-6197

Received 15 April 2019; Accepted 8 January 2020

Journal of Experimental Biology (2020) 223, jeb204438. doi:10.1242/jeb.204438

MON is found in the majority of anamniotic vertebrates, where it is the primary termination site for lateral line neuromast afferents (New et al., 1996). Neuromasts are distributed either on the surface of the skin or within sub-dermal canals (Fig. 1A). The sole efferent cell type of the MON, which projects to the midbrain, is the ascending efferent neuron (AEN; in some species these are called crest cells) (Fig. 1B) (Boord and Northcutt, 1982). Basilar AEN dendrites are contacted by primary afferent fibers of lateral line neuromasts that form a somatotopic map in the deep layers of the MON (Bodznick and Northcutt, 1980; Bodznick and Schmidt, 1984). Spine-covered apical AEN dendrites extend into an overlying molecular layer where they are contacted by highly numerous inputs from the thin, unmyelinated axons of granule cells. These axons course long distances through a molecular layer, similar to the parallel fibers in the molecular layer of the cerebellar cortex. Parallel fibers arise from granule cells in the lateral granular area (continuous with the granule cell mass that gives rise to the parallel fibers of the electrosensory molecular layer in these fish) (Schmidt and Bodznick, 1987). The parallel fiber system is thought to convey corollary discharge as well as proprioceptive input signals to the AENs.

As in the electrosensory and auditory systems, responses of mechanosensory receptors to reafference generated by movements (such as those associated with ventilation or swimming) can obscure the response to externally generated signals of interest. Unlike electroreceptors, lateral line mechanoreceptors receive inhibitory efferent innervation (Roberts and Russell, 1972; Russell, 1971). This could reduce reafference by turning off the receptors during behavior, but the efferents appear only to be activated during very vigorous behaviors that threaten to overdrive receptors (Bodznick, 1989; Roberts and Russell, 1972). The requisite movements of behaviors such as ventilation and swimming cause self-stimulation that drives lateral line primary afferent responses (Montgomery et al., 1996; Russell and Roberts, 1974; Palmer et al., 2005; Ayali et al., 2009; Mensinger et al., 2018). However, second-order cells are not driven by the same self-stimulation, at least in the case of ventilation (Montgomery et al., 1996). In theory, inhibitory motor-related signals could gate out brief, stereotyped reafferent input to second-order cells; however, many behaviors (such as swimming and ventilation) generate ongoing self-stimulation. Prolonged inhibition during these ongoing behaviors seems unlikely as responses to important external stimuli would be inhibited as well. A recent study in toadfish indeed found that the lateral line system remains sensitive to external stimuli in spite of self-stimulation generated by swimming (Mensinger et al., 2018). It appears that a more dynamic filter would be useful under most circumstances and evidence for predictive cancellation of reafference was briefly reported in the MON of the teleost scorpion fish, but this has not been further studied (Montgomery and Bodznick, 1994).

Here, we set out to test further the hypothesis that the cerebellum-like circuitry of the MON supports the generation of predictions for expected sensory input based on movement-related signals (Fig. 2A). We recorded the spiking activity of AENs in the MON of an elasmobranch fish, the skate (*Leucoraja erinacea*), while manipulating the relationship between external stimuli and signals associated with the animal's own movements (Fig. 2B). We found that AENs reduce their response to external stimuli time-locked to movement-related signals and demonstrate negative images of such expected sensory-driven responses. Critically, we found that negative image formation depends on coupling between the sensory stimulus and movement-related signals and is not observed in the spiking responses of afferent input to AENs. Together, these results support the model of a conserved computation implemented by cerebellum-like circuits across vertebrates.

MATERIALS AND METHODS

Animals and surgery

For all experiments we used adult, wild-caught little skates, *Leucoraja erinacea* (Mitchill 1825), of either sex; a total of 19 skates were used in

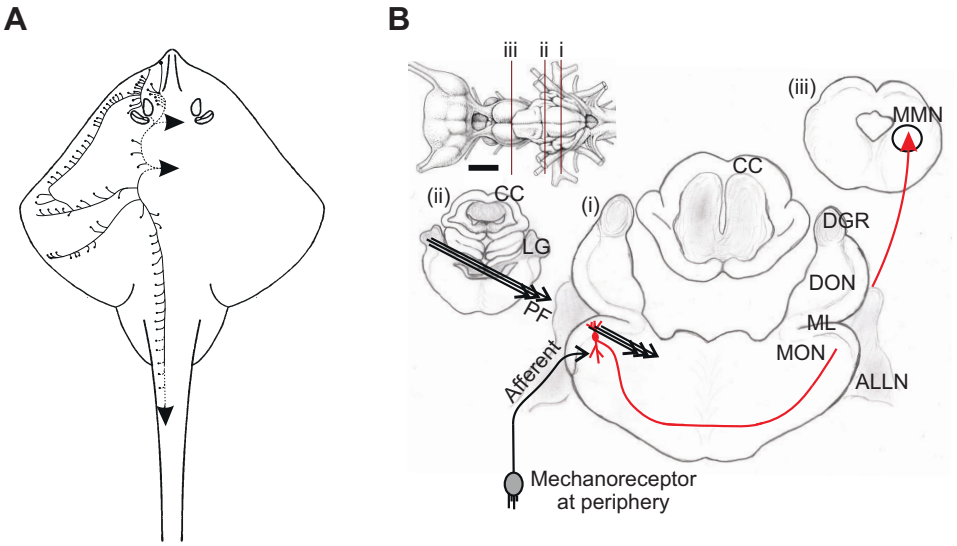

Fig. 1. Lateral line system and the central connections of the cerebellum-like nucleus. (A) A drawing of the lateral line canals on the dorsal side of the skate. Canals were visualized by injection of Cobalt Blue at intermittent locations along the canal. Canals are represented by lines and terminate in dots, which denote canal pores. Dotted lines denote inferred continuity between well-visualized segments of canal. (B) Diagram of the pathway for connections to/from the medial octavolateral nucleus (MON) across three representative coronal sections (i–iii) of the brain (not to scale). A cartoon AEN is shown with its apical and basal dendrites and its axon colored in red. Parallel fibers (PF) originate from granule cells in the lateral granular (LG) area and course through the molecular layer (ML) of the MON. Mechanosensory afferents enter the MON via the anterior lateral line nerve (ALLN). CC, corpus cerebelli; DGR, dorsal granular ridge; DON, dorsal octavolateral nucleus.

Journal of Experimental Biology (2020) 223, jeb204438. doi:10.1242/jeb.204438

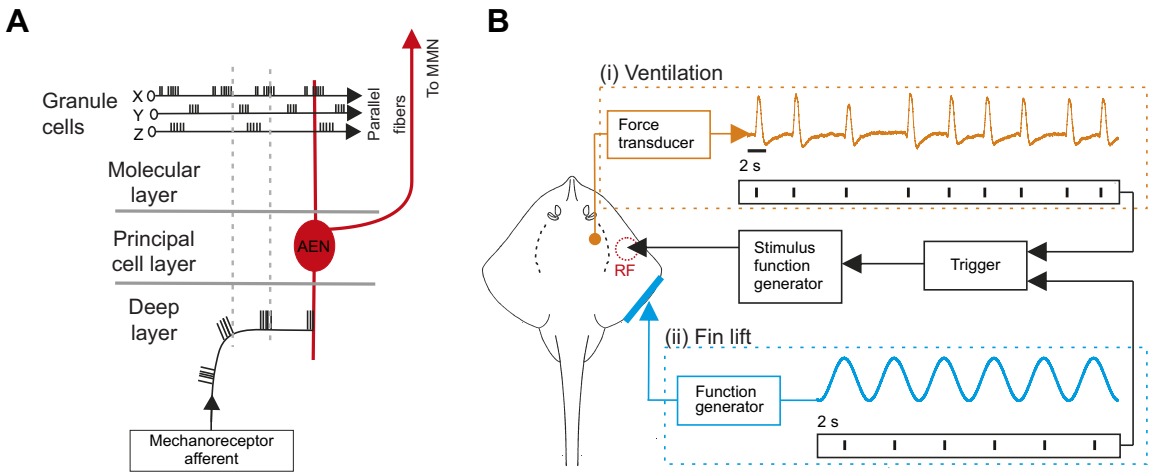

Fig. 2. Cerebellum-like circuitry of the medial octavolateral nucleus (MON). (A) A laminar organization featuring a parallel fiber molecular layer is shared by all cerebellum-like structures. In the MON, ascending efferent neuron (AEN) cell bodies are situated in the principal cell layer. According to previous work on the electrosensory system, a cancellation signal at the parallel fiber inputs would be generated by a decorrelation learning rule between sensory afference and granule cell activity. Only the subset of parallel fiber inputs active at the same time as excitatory afferent input (X) would be depressed and would cancel the response to future coincident afferent input. Responses to afferent input uncorrelated with parallel fiber activity (Z and Y) would remain unaffected and be conveyed to the medial mesencephalic nucleus (MMN). (B) Schematic diagram illustrating the experimental set up for synchronizing stimulus delivery with either of the two different movement-related signals used in this study: (i) orange – the respiratory movements of ventilation (measured with a force transducer) that would be associated with proprioceptive or corollary discharge signals; and (ii) blue – externally imposed sinusoidal movements of the fin that provide proprioceptive signals or spatially broad mechanosensory reafference (available during behaviors such as swimming). A mechanosensory stimulus was presented (triggered by each phase of one of these two signals) to the receptive field (RF; dashed red circle) of the recorded cell to modulate its spiking activity (not shown).

this study. Animals were obtained from the Long Island Sound and housed in local facilities at Wesleyan University (Middletown, CT, USA) or Marine Biological Laboratories (Woods Hole, MA, USA). Skates were group housed (no more than 6 fish per cubic meter of water) in tanks at around 12–14°C (either artificial seawater or natural seawater) and maintained on a daily diet of squid. For all experiments, animals were first anesthetized by immersion in 0.04% benzocaine and surgical procedures were performed as previously described (Duman and Bodznick, 1996). The brains were exposed by removal of the overlying cartilage, and decerebrated by diencephalic section. The skates were either fully paralyzed by injection with tubocurare (0.1 mg kg^{-1} i.v., Sigma), to allow the manipulation of body posture, or partially paralyzed by destroying the spinal cord to eliminate trunk and tail movements but leave normal breathing movements intact (for the ventilation experimental condition as described below). After surgery, the fish were transferred to a Plexiglas experimental tank of cold seawater (9°C), and positioned with a Plexiglas head holder so that the cranial opening was just above the water surface. A gentle flow of seawater (0.1–0.4 l min^{-1}) was directed into the mouth as an extra support to ventilation. All procedures followed NIH guidelines for the care and use of experimental animals and were approved by the Animal Care and Use Committees of Wesleyan University and the Marine Biological Laboratory.

Electrophysiological methods

AEN unit activity was recorded extracellularly using Pt black-tipped indium electrodes (2–7 MΩ, 1–2 µm tip), which provided a high signal-to-noise ratio for single unit isolation in this region. Afferent unit activity was recorded extracellularly using pulled sharp glass electrodes (20 MΩ) filled with 4 mol l^{-1} NaCl. All neural signals were filtered, amplified and then acquired using Cambridge Electronic Designs 1401 ADC and Spike2 software (CED, Cambridge, UK).

The mechanosensory MON is located ventral to the electrosensory dorsal octavolateral nucleus (DON) in skates (Fig. 1B). Recordings of individual AENs in the MON were targeted by first identifying surface landmarks characteristic of the DON and then advancing the electrode (perpendicular to the dorsal surface) until responses to an electrosensory dipole stimulus ceased. Once in the MON, the electrode was slowly advanced until well-isolated spikes were detected on the oscilloscope trace of the raw waveform (this signal was also monitored acoustically by sending it through a speaker). All AENs were positively identified by their short-latency (2–3 ms) antidromic activation by electrical stimulation of the contralateral medial mesencephalic nucleus (MMN), which is the AEN target region located in the caudal mesencephalon just rostral to the corpus cerebellum (Fig. 1B). The AENs in the MON respond to mechanosensory but not electrosensory stimuli, which provided additional confirmation of identity.

Mechanosensory afferents were recorded with sharp glass electrodes placed in the intracranial portion of the posterior lateral line nerve before its point of entry into the hindbrain. Mechanosensory afferents were identified by their robust responses to mechanosensory stimuli and lack of responses to electrosensory stimuli.

Experimental procedures

Throughout the study, the experimental unit was a single cell (AEN or afferent) from which spiking activity was continuously recorded. Each experiment comprised trials that were split into three main periods (Fig. 3A): (1) a prestimulus period; (2) a stimulus period during which a local mechanosensory stimulus was triggered by trial onset; and (3) a poststimulus period. Throughout each experiment, single trials were triggered by either: (1) signals associated with the animal's own movement/behavior (paired condition) or (2) an internal clock (freerun condition). Five out of 27 AENs were stable enough to be recorded under both the paired and the freerun experimental condition (as reported in Results); 22/27 AENs were recorded only in the paired experimental condition. To trigger trial onset for each experiment in the paired condition, we used either: (1) the respiratory movements of ventilation or (2) externally imposed swimming movements of the fin that could

Journal of Experimental Biology (2020) 223, jeb204438. doi:10.1242/jeb.204438

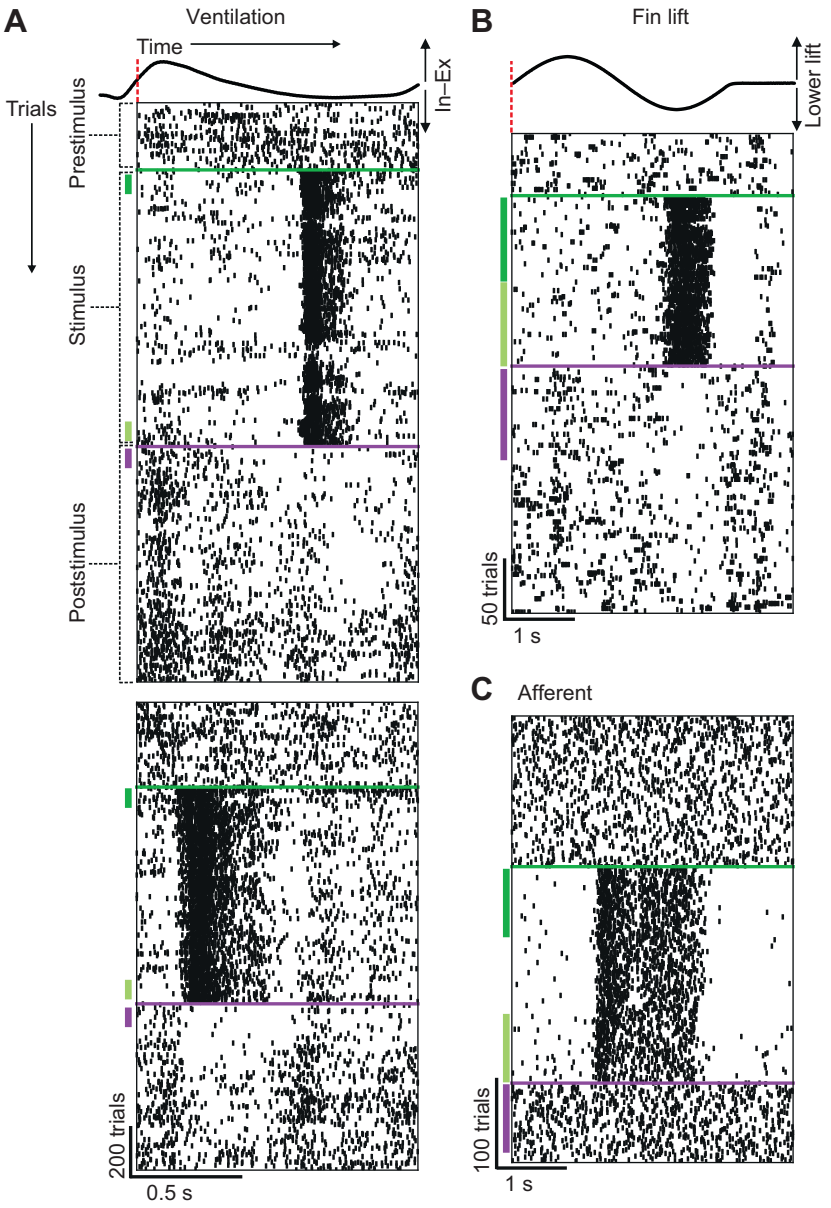

Fig. 3. Experimental design and example data. (A) Raster display of the spiking activity (each spike is a tick mark) of an AEN during a paired experimental condition in which each trial (row) is triggered by the respiratory movements of ventilation. The average inhalation–exhalation (In–Ex) cycle on each trial is plotted above the raster and the trial onset at t=0 is denoted by a red line. An experiment has three periods as labeled in the top panel: prestimulus, stimulus and poststimulus. During the stimulus period, a mechanosensory stimulus is presented on each trial that modulates spiking activity (initial stimulus period indicated by the dark green vertical bar; final stimulus period indicated by the light green vertical bar). Removal of the mechanosensory stimulus at the end of the stimulus period reveals a spiking pattern in the initial trials of the poststimulus period (vertical purple bar) that looks like a negative image of the stimulus-driven response. Later in the poststimulus period, spiking activity again resembles that in the prestimulus period. The bottom panel shows a second iteration of the pairing experiment, which was performed in the same cell, in which the stimulus and the corresponding stimulus-driven spiking response were shifted in phase relative to trial onset. It appears that, in each pairing experiment, the phase of the negative image is specific to the phase of the stimulus-driven response. (B) Same as the top panel of A, but for a pairing experiment in a different AEN in which each trial was triggered by the onset of the externally imposed fin lift cycle (top trace above raster). (C) Same as in B but for an afferent fiber.

provide proprioceptive signals or spatially broad mechanosensory reafference related to behaviors such as swimming (Fig. 2B).

We monitored the respiratory movements of ventilation with a force transducer placed against the skin over the branchial chamber in partially paralyzed skates. Externally imposed (passive) fin movements were generated in fully paralyzed skates by attaching a soft plastic clamp to the ipsilateral pectoral fin, which was then connected to an arm extending from a servo motor slaved to a sinusoidal function generator and triggered by an internal clock.

Each ventilation cycle had a median period of 2.93 s (interquartile range, IQR 1.96–3.62 s; n=21 paired experiments in 21 AENs). In experiments in which the fin was artificially raised and lowered to mimic swimming movements, the fin lift interval (triggered by an internal clock) was set to a slightly longer duration of 4–6 s to minimize turbulent water disturbance (n=6 paired experiments in 6 AENs). The speed and amplitude of artificial fin lifts were titrated to avoid excessive modulation of baseline spike rates in AENs, which were 1.8 Hz (1.5–2.4 Hz) for the 6 AENs in this condition. AEN spike rates were 1.5 Hz (1.1–2.3 Hz; n=21 cells) under the ventilation condition. The difference in baseline firing rates between these two experimental conditions was not significant (Mann–Whitney U=55; P=0.33; n_1=21 AENs in ventilation condition and n_2=6 AENs in fin lift condition).

All cells used in this study had receptive fields localized to the dorsal surface of the skate. During the stimulation period, a mechanosensory stimulus was delivered by either a touch of the skin with a small rod or a small steady stream of water directed toward the skin surface. The stimulus was attached to an arm extending from a servo motor slaved to a sinusoidal function generator. A single sinusoidal cycle was triggered by the onset of each trial such that on each trial the stimulus moved into and then back out of the receptive field of the single unit being recorded. To test the main hypothesis of this study, we chose whichever method (water flow or touch) elicited maximal AEN spike rate modulation from the recorded AEN and we did not distinguish between these two variations of stimulus delivery in the results. We know from extensive work in the electrosensory systems that, although coincident activity is a requirement for changes in molecular layer synaptic strength

underlying the adaptive filter mechanism, the results do not qualitatively differ based on the way in which spiking responses are evoked. Even direct intracellular current injection provides changes in spiking that are sufficient for the generation of cancellation signals (Bell et al., 1997c; Bodznick et al., 1999; Bertetto, 2007; Zhang and Bodznick, 2010; Kennedy et al., 2014; Muller et al., 2019).

Experimental period, duration and number of trials

As described above, each experiment with an AEN included three periods (prestimulus, stimulus and poststimulus; Fig. 3A). Each period included a varying number trials and inter-trial intervals. In the ventilation-triggered paired experimental condition, the inter-trial interval varied during each experiment because trial onset was determined by the animal's own behavior. However, for analysis purposes, the trial duration was set to a constant value across trials in a single experiment. During the stimulation period, the mechanosensory stimulus was triggered by trial onset and moved into and then out of the receptive field of the recorded neuron. The period of this stimulus movement itself often approached the duration of the inter-trial interval. Additionally, water movement in the tank following mechanosensory stimulation continued to modulate spiking activity and meant that stimulus offset could not be well defined by the cessation of the overt stimulus movement. For each cell, the spiking response window was triggered at trial onset and the response duration was set as the average period of modulated spiking for the cell, which varied from cell to cell and with the different stimuli used. Across paired experiments, the median trial duration used was 1.5 s (1–6 s; n=33 paired experiments in 33 cells – afferents and AENs).

For different experiments, there was also some variability in the number of trials per period due to such things as the stability of the recording. During the prestimulus period, all recorded trials were used to get an estimate of the prestimulus spiking response. The number of prestimulus trials obtained for each experiment ranged from 12 to 425 with a median 117 (76–189 IQR; n=44 experiments in 36 cells – afferents and AENs). The 'initial' and 'final' stimulus-driven spiking responses were estimated using the first 75 and the last 75 trials of the stimulus period, respectively (dark green and light green vertical lines in Fig. 3A). The poststimulus spiking response was estimated using the first 75 poststimulus trials (purple vertical line in Fig. 3A). Results were qualitatively the same whether we performed analyses using 50, 75 or 100 trials to estimate the responses in each period. In 6 out of 44 total experiments (one in each of 6 different cells), the cell was not held long enough to obtain 75 trials in the poststimulus period; for these experiments, all trials in the poststimulus period were used to estimate the poststimulus spiking response. In 8 out of 44 total experiments (one in each of 8 different cells), the stimulus period was shorter than 150 trials; for these experiments, the stimulus period was divided in half to estimate the initial and final stimulus spiking responses. Across all 44 experiments (conducted in 36 total cells – afferents and AENs), the number of trials in the stimulus period ranged from 91 to 1051 with a median of 224 trials (188–346 IQR).

Data processing and analysis

Spike times

Spike times were extracted from raw recordings and all analyses were performed using custom-written scripts for Python (data and custom written analysis routines formatted for Python Jupyter Notebook are available via the open source repository G-Node (doi:10.12751/g-node.879051). For 24 out of the total 27 recorded AENs and all 9 recorded afferents, the signal-to-noise ratio of the raw signal was high enough that simple peak detection was enough to extract all spike times. For three of the AENs, level detection alone was insufficient and SpyKING CIRCUS (Yger et al., 2018; an open source Python platform for spike sorting) was instead used to extract spike times.

Spiking responses

The critical test of the central hypothesis is whether and how spiking responses changed during and after the stimulation period. For each trial, we quantified the spiking responses in two ways: (1) as an average spike rate (as described in Results) and (2) as an instantaneous spike density function. For a given cell, we then averaged across trials within a given period of an experiment to get the trial-averaged spiking response for that period within that experiment. To calculate the spike density functions, we convolved the spike train on each trial with a normalized Gaussian kernel. The bandwidth of the kernel was optimized to spiking activity during the prestimulus period using standard analytical methods (Shimazaki and Shinomoto, 2010). The optimum Gaussian kernel bandwidth (tau) for AEN experiments was 0.06 (0.042–0.077 IQR; n=35 experiments in 27 cells) and for afferents it was 0.06 (0.042–0.198 IQR; n=9 experiments in 9 cells).

Statistics

The results reported in this study were obtained by analyzing data from a total of 27 individual AEN units (from 16 skates) and 9 individual afferent units (from 3 skates). From individual skates, 1–4 AENs were recorded and 2–3 afferents were recorded. AENs and afferents were not recorded in the same skate. When multiple units were recorded from the same animal they were often recorded on different days, sometimes several days apart. Individual neurons are considered independent samples in this study. Data are never grouped by animal identity and we did not test animal identity as a factor in any of the effects reported here.

All 27 AENs were tested in the paired experimental condition. Some additional experimental conditions discussed in Results were only achieved in a subset of the AENs. For all comparisons and summary statistics presented here, we report the exact number of cells tested in the given condition. For each comparison, the number of experiments equals the number of cells unless explicitly stated otherwise. Throughout the text, population data are summarized as the median (50% quantile) and IQR (25%–75% quantiles), again with a value 'n' reporting the sample size of the specific set of cells in question.

As discussed in the Introduction, the central hypothesis of this study was that the cerebellum-like circuitry of the MON enables AENs to generate a cancellation signal to afferent mechansensory stimulation when the afferent input is time locked to the skate's own movements/behavior. This cancellation signal would be revealed through: (1) changes in the AEN poststimulus spiking response relative to the prestimulus response (or negative image); and (2) changes in the final stimulus-driven response compared with the initial stimulus-driven response. Therefore, we have defined in advance this set of planned within-cell comparisons. Absolute effect sizes are reported throughout. For within-cell comparisons, we tested the statistical significance of effect sizes using the two-tailed Wilcoxon signed-rank test. Results were considered significant if the statistical test returned a P-value <0.05 (unless a different criteria is explicitly stated otherwise). For each two-tailed within-cell comparison, we report the raw W test statistic. For sample sizes >15, we report the P-value calculated by the

approximate standard normal distribution. For sample sizes <15, the approximate standard normal distribution is no longer accurate and we instead report the critical W value at α=0.05 for the given sample size (with a value 'n' reporting the sample size of the population in which the given comparison is being made).

We report the results of non-parametric tests throughout due to overall small sample sizes and the failure of some of the reported data distributions to pass the test of normality (D'Agostino's K^2 test result at P<0.05). All of the reported data distributions were homoscedastic (Bartlett's test for equal variances; all results P>0.47).

Graphical representations of the data/results were generated in custom Python routines and saved directly to .eps files. These vectorized graphics were then imported to Corel Draw for construction of the final figures as shown. Scripts used to generate the original images were written in open source software and are available upon request or via G-Node (doi:10.12751/g-node.879051).

RESULTS

We hypothesize that the cerebellum-like circuitry of the MON enables AENs to generate cancellation signals for predictable sensory input that is associated with the movements of behaviors (Montgomery and Bodznick, 1994; Bodznick et al., 1999; Hjelmstad et al., 1996; Schmidt and Bodznick, 1987). To test this central hypothesis, we examined whether spiking responses changed during and after a period of repeated stimulus presentation paired with movement-related signals. Under this 'paired' experimental condition (see Materials and Methods for more details), a cancellation signal would be revealed through: (1) changes in the AEN poststimulus spiking response relative to the prestimulus response; and (2) changes in the final stimulus-driven response compared with the initial stimulus-driven response. We examined changes in the magnitude of the spiking response and the temporal specificity of these effects.

Throughout each experiment in the paired condition, trial onset was triggered by one of two signals associated with ventilation or swimming movements (Fig. 2B; as described in Materials and Methods). Based on previous literature in the electrosensory system, proprioceptive signals and motor commands associated with both ventilation and proprioceptive signals and sensory feedback signals associated with fin movements are expected to provide a basis for the generation of cancellation signals (Schmidt and Bodznick, 1987; Montgomery and Bodznick, 1994). An example cell from each condition is shown in Fig. 3A,B. Overall, the results obtained under these two conditions were not significantly different from each other (by two-tailed Mann–Whitney test; n_1=21 AENs in ventilation condition; n_2=6 AENs in fin lift condition) and have been combined for all analyses (though group identity is indicated for visualization in figures). In the prestimulus period, AENs had very low spike rates of 1.6 Hz (1.2–2.4 Hz; n=27 cells). During the stimulus period, we introduced a mechanosensory stimulus triggered by the onset of each trial. In general, spiking activity appeared to be modulated throughout much of the duration of each trial during this period (see example cells in Figs 3 and 5). We first averaged across each trial to get an estimate of the trial spike rate during each experimental period for each cell (as described in Materials and Methods). Stimulation significantly increased AEN spike rates by 1.7 Hz (0.8–2.7 Hz; n=27 cells) in the initial stimulus period relative to the prestimulus period (W=8; P<0.001; n=27 cells) (Fig. 4A).

After repeated pairing of the stimulus with a behavioral cue, we found, first, that the stimulus-driven response in AENs had decreased significantly during the stimulus period by 0.5 Hz (0.9–0.1 Hz) (Fig. 4A; W=98; P=0.03; n=27 cells), though spike rate was still elevated by 1.1 Hz (0.3–1.8 Hz) compared with that in the prestimulus period (W=17; P<0.001; n=27 cells). Second, when we then withheld the stimulus, the AEN spike rate in the poststimulus period decreased significantly relative to that in the prestimulus period by 0.3 Hz (0.7–0.1 Hz) (Fig. 4A; W=80; P=0.009; n=27 cells). This effect is also readily observed in the example spike rasters depicted in Figs 3 and 5. These results are consistent with the generation of a cancellation signal, and are not likely explained by changes to afferent input. Afferents fired more regularly than AENs in the prestimulus period at 7.4 Hz (2.1−15 Hz; n=9). As shown in the example cell of Fig. 3C, the mechanosensory stimulus modulated afferent spiking activity. However, when averaged across each trial, afferent spike rate was not changed significantly either by the stimulus or during or after the stimulus period (data not shown). Based on extensive work on the adaptive filter model in the electrosensory and auditory systems, it is expected that this observed change in AEN responses after the stimulus period would depend on coupling between the stimulus and a movement-related signal (conveyed by parallel fiber inputs to AENs) (Bell et al., 1981; Bodznick et al., 1999; Zhang and Bodznick, 2008; Singla et al., 2017). For a subset of these AENs (n=5/27 cells), we performed an additional iteration of the experiment in which the trials were yolked to an internal computer clock ('freerun' condition) rather than the animal's own behavior. Only in the paired condition did all five AENs exhibit decreased spike rates in the poststimulus period relative to the prestimulus period (Fig. 4B; same cells as those in the analysis corresponding to Fig. 5D) (paired condition: W=0; critical W at P<0.05=0 for n=5 cells; freerun condition: W=7: critical W at $\alpha_{0.05}$=0 for n=5 cells). Specifically, the poststimulus spike rates were lower in the paired relative to the freerun condition in 4/5 of these cells. Together, these results are consistent with the development of a cancellation signal for the stimulus-driven response as a result of stimulus pairing with movement-related signals. However, changes to the overall spike rate of AENs could be explained by other factors such as neural fatigue. Although a comparison between freerun and paired conditions would rule out this alternative explanation of the results, with a sample size of n=5 it is difficult to make a strong conclusion from this result alone. Importantly, changes to the temporal profile of the AEN spiking response are equally as important as changes in its magnitude when assessing the generation of a cancellation signal/negative image.

Temporal specificity is an important component of predictive cancellation via an adaptive filter mechanism that distinguishes it from other potential non-plastic gating mechanisms. In the adaptive filter mechanism, the cancellation signal should be specific to the phase of the stimulus response relative to the onset of a movement or behavior. As observed in the example spike raster plots (Figs 3 and 5), the stimulus-driven responses were inhomogeneous in time yet specific, with a repeatable unique temporal profile. For example, Fig. 3A shows data from an AEN in which we were able to repeat a second iteration of the pairing experiment in which the phase of the stimulus-driven response was explicitly shifted by shifting stimulus onset on each trial. As seen in this example cell, the shift in the phase of the stimulus response resulted in a similar shift in the phase of a temporally patterned poststimulus response. This behavior would be consistent with predictive cancellation by an adaptive filter mechanism, but not with other mechanisms such as fixed gating by inhibitory efference. Importantly, time-locked changes in the temporal profile of the post-stimulus spiking response that are specific to the phase of the stimulus-driven response cannot be

Journal of Experimental Biology (2020) 223, jeb204438. doi:10.1242/jeb.204438

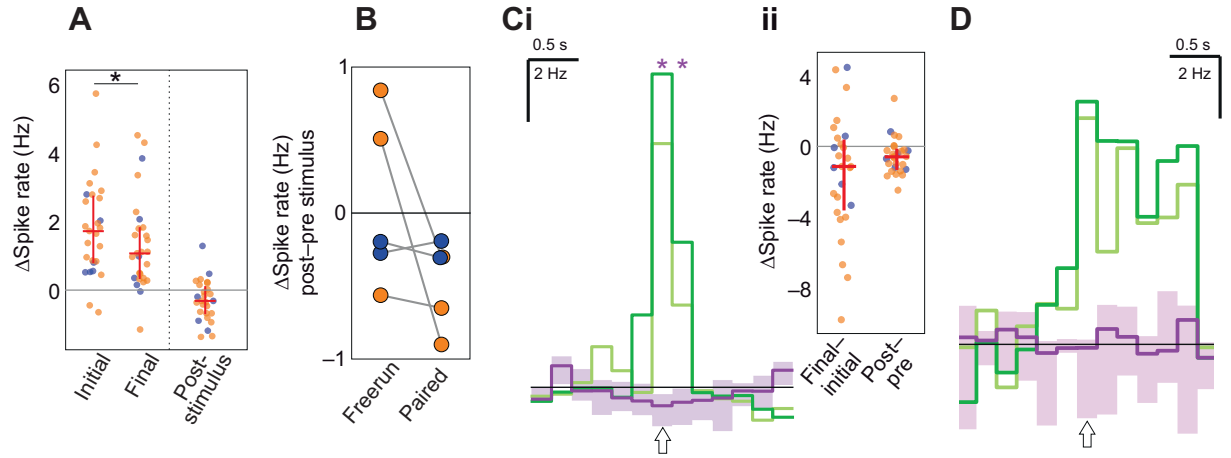

Fig. 4. Stimulus pairing induces changes in AEN spike rates that oppose the stimulus response. (A) Scatter plot of the spike rate in each of 27 AENs in the paired experimental condition during the stimulus period (initial and final) and the poststimulus period. Spike rates are relative to those in the prestimulus period for each cell. Data are colored by the trigger source (orange, ventilation; blue, fin lift). Red lines depict the median (the location of the horizontal line on the *y*-axis) and the interquartile range (IQR: Q1–Q3; the span of the vertical line) of each distribution. Spike rates in all stimulus periods (initial, final, post) were significantly different from prestimulus rates (P<0.05; n=27; Wilcoxon two-tailed within-cell comparisons as described in Results). Mechanosensory stimulation drove a net increase in spike rate that declined over the course of pairing (asterisk indicates significance at P<0.05 by the Wilcoxon two-tailed test between the final and initial stimulus period as described in Results). Critically, AEN spike rate decreased significantly in the early poststimulus period, which is consistent with the generation of a cancellation signal for the stimulus-driven response. (B) Scatter plot showing data from the five AENs in which both a paired and a freerun experiment were conducted in the same cell (these are a subset of the 27 cells shown in A). Spike rates in 4/5 of these AENs were more decreased in the paired versus the freerun experimental condition (same cells as those shown in Fig. 5D; orange, ventilation triggered; blue, fin lift triggered). The poststimulus rates were significantly different from the prestimulus rates in the paired condition (poststimulus rates were reduced in all 5/5 of these AENs in the paired condition; W=0 by Wilcoxon two-tailed test; critical W at $\alpha_{0.05}$=0 for n=5). (C) Changes in poststimulus spike rate were temporally specific (and opposed) to changes in stimulus-driven spike rate. (i) Histogram of the mean trial-averaged spike rate of AENs (200 ms bins) in each period (dark green, initial stimulus period; light green, final stimulus period; purple, poststimulus period; purple shading denotes the IQR for poststimulus responses in each bin) (n=27 cells). For each cell, the trial-averaged prestimulus spike rates were subtracted and responses were aligned at t=0 (arrow) to the bin in which the maximum stimulus-driven response was evoked. Bins in which the poststimulus spike rate was significantly decreased relative to prestimulus rate are indicated by an asterisk (P<0.001; Wilcoxon two-tailed within-cell comparisons as described in Results). (ii) Scatter plot of the population data corresponding to the center bin (arrow in i) (n=27 cells). Spike rates decreased significantly over the course of stimulus pairing (final−initial) and spike rates were significantly decreased in the poststimulus period relative to the prestimulus period (post−pre). (D) Same as in C but for the afferent population (n=9 cells). Poststimulus spike rates were not different from prestimulus rates in any of the bins. For all comparisons in A–D, individual cells are considered independent samples. For each condition (paired or freerun; ventilation or fin lift), data are from one experiment per cell.

explained by generalized synaptic or neural fatigue. We were only able to achieve an explicit phase-shifted iteration of the experiment in two of the total 27 AENs. However, we implemented two analytic methods to assess the temporal specificity of cancellation signals in all of the 27 AENs of the study.

First, to examine whether the observed poststimulus changes in AEN spike rate (Fig. 4A) preserved the temporal specificity of the stimulus-driven response, we estimated the trial-averaged spike rate per 200 ms bin in each period of the experiment in each cell (Fig. 4C,D). We then aligned responses across cells according to the bin in which the maximum stimulus-driven spike rate was evoked. In the stimulus period, spike rate in this center bin was initially 10 Hz (6.3–13 Hz; n=27 cells) above prestimulus rate (W=0; P<0.001; n=27 cells). Consistent with the previous results, the peak stimulus-driven spike rate decreased significantly by 1.1 Hz (3.5–0.3 Hz; n=27 cells) by the end of the stimulus period (Fig. 4C; center bin: W=96; P=0.025; n=27 cells). As would be predicted by a temporally specific cancellation mechanism, we found that the poststimulus response was decreased relative to the prestimulus response only in the bins including and immediately surrounding the peak stimulus-driven response [Fig. 4C; center bin: −0.6 Hz (−1.2 to −0.2 Hz); W=65; P=0.003; n=27 cells]. Across the afferent population, peak stimulus-driven spike rate was also significantly elevated above prestimulus rate by 7.7 Hz (7.3–9.9 Hz) in the center bin (W=0; critical W at $\alpha_{0.05}$=6 for n=9; Fig. 4D). However, this response did not decrease significantly by the end of the stimulus period (center bin: −1.7 Hz, −2.6 to −0.3 Hz; W=9; critical W at $\alpha_{0.05}$=6 for n=9). Finally, unlike AENs, afferents exhibited no difference between the poststimulus spiking response and the prestimulus spiking response in this (or any other) bins [Fig. 4D; center bin: −0.1 Hz (−2.4 to 0.2 Hz); W=17; critical W at $\alpha_{0.05}$=6 for n=9]. These results indicate that changes in AEN spike rate cannot be accounted for by changes in the afferent input. These results are consistent with the generation of a cancellation signal within AENs themselves.

The adaptive filter cancellation mechanism achieves temporal specificity as a result of the decorrelating effects of anti-Hebbian plasticity with relatively high temporal precision. Consequently, as shown extensively in the electrosensory systems, poststimulus spiking responses are negatively correlated with stimulus-driven responses after a period of stimulus pairing with movement-related signals. The negatively correlated poststimulus response is therefore termed the negative image (Bell et al., 1981; Montgomery and Bodznick, 1994; Bastian, 1996). The analysis in Fig. 4C reveals coarsely that, at a population level, the poststimulus response is negatively correlated with the stimulus-driven response in the population of MON AENs examined here. We examined this more directly and with higher temporal resolution on a cell-by-cell basis by testing whether the poststimulus spiking response was more negatively correlated with the stimulus response than the prestimulus response had been.

We preserved the pattern of spike times by estimating an instantaneous spike density function (Fig. 5A,B; refer to Materials and Methods for more detail). We then measured the Spearman's

Journal of Experimental Biology (2020) 223, jeb204438. doi:10.1242/jeb.204438

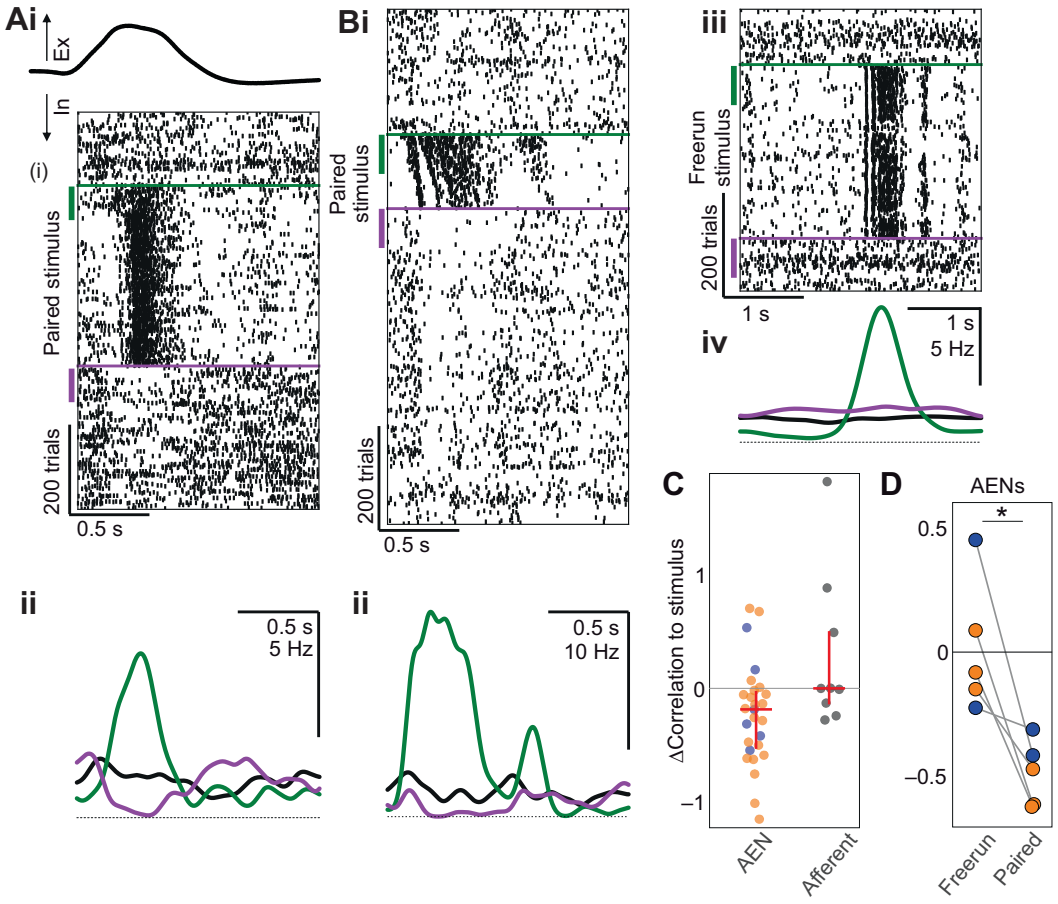

Fig. 5. AENs generate negative images to stimulus responses that are paired with movement-related signals. (Ai) As in Fig. 3, raster display of AEN spiking under the paired experimental condition triggered by the ventilatory movements (top trace). (ii) Smoothed trial-averaged spiking response plotted for each period [black, prestimulus; green, stimulus (initial); purple, poststimulus; see Materials and Methods for details]. Dotted line denotes a spike rate of 0 Hz. Note: poststimulus activity resembles a negative image (inverse) of the stimulus-driven response and approaches 0 Hz during the time the stimulus-evoked response was strongest. (Bi,ii) Same plots as in A but for a different AEN. (Biii,iv) Same AEN as in i and ii, but under the freerun experimental condition in which each trial is triggered by a regular clock interval (desynchronized from ventilation). Under this freerun condition, the poststimulus response is similar to the prestimulus response. (C) For AENs, but not afferents, the stimulus response tended to be more negatively correlated with the poststimulus response than with the prestimulus response (orange, ventilation trigger; blue, fin lift trigger). Scatterplot of the data for all AENs (n=27 cells) and for all afferents (n=9) tested in the paired experimental condition (change in correlation to stimulus=poststimulus:stimulus correlation minus prestimulus:stimulus correlation). There was a significant change for AENs (P<0.05; n=27; Wilcoxon two-tailed within-cell comparisons as described in Results). (D) Scatter plot of the change in stimulus correlation for the paired and the freerun experimental condition in the subset of 5/27 AENs tested under both conditions (same cells as those shown in Fig. 4B; orange, ventilation trigger; blue, fin lift trigger). Asterisk denotes a significant effect of experimental condition (in all 5/5 of these AENs, the poststimulus response was more negatively correlated to the stimulus response in the paired versus the freerun condition; W=0 by Wilcoxon two-tailed test; critical W at $\alpha_{0.05}$=0 for n=5). The poststimulus correlation was significantly different from the prestimulus correlation in the paired condition (the poststimulus correlation was reduced in all 5/5 of these AENs in the paired condition; W=0 by Wilcoxon two-tailed test; critical W at $\alpha_{0.05}$=0 for n=5). For all comparisons in C and D, individual cells are considered independent samples. For each condition (paired or freerun; ventilation or fin lift), data are from one experiment per cell.

correlation between (1) the prestimulus response and the stimulus response and (2) the poststimulus response and the stimulus response. Within each cell, we compared the correlation between the poststimulus response and the stimulus response with the correlation between the prestimulus response and the stimulus response. In the paired condition, just as predicted by the adaptive filter model, AENs had a poststimulus response that was more negatively correlated with the stimulus response than it was with the prestimulus response [Fig. 5C; difference in correlation=−0.18 (−0.52 to −0.03); W=80; P=0.009; n=27 cells]. Afferents exhibited no change in the correlation with the stimulus response between the poststimulus and prestimulus periods [Fig. 5C; difference in correlation=0 (−0.13–0.5); W=18; critical W at $\alpha_{0.05}$=8 for 9 cells]. For the subset of AENs tested in both the paired and the freerun experimental condition (5 out of the 27 AENs), the poststimulus response was more negatively correlated to the stimulus response in the paired condition than in the freerun condition in all 5/5 cells (Fig. 5D; W=0; critical W at $\alpha_{0.05}$=0 for n=5; same 5 cells as those in the analysis corresponding to Fig. 4B). Under the freerun condition, the AENs were prevented from forming their negative image of the stimulus response. In other words, yoking an external stimulus to a behavioral signal led to a post-pairing response in AENs that was like a negative image of the stimulus response, and this effect was specific to the AEN population. Importantly, a time-locked change in the 'shape' (temporal profile) of the post-pairing spiking response that mirrors the stimulus-evoked response cannot be explained by fatigue.

Together, these results are consistent with a model in which anti-Hebbian plasticity enables the parallel fiber system to act as an adaptive filter, tuned through experience, to form a forward model

of the reafference, also termed a cancellation signal, that cancels AEN responses to the reafference without gating out sensory input from other sources.

DISCUSSION

The central nervous system of all major groups of craniates except reptiles and birds includes both a cerebellum and structures with circuitry that is similar to the cerebellum. As described in numerous papers and reviews, studies of electrosensory cerebellum-like structures have provided a relatively clear mechanistic account of how this circuitry can learn predictions of sensory reafference based on a variety of central reference signals and then use those predictions to cancel responses to reafference from the system (Bell et al., 1997a, 2008; Sawtell, 2017). That the stereotyped cerebellum-like circuit performs this function in phylogenetically well-separated as well as independently evolved electrosensory systems suggests that the cerebellum-like circuit is what endows this fundamental computation to these structures (Bullock et al., 1983). Consistent with this, recent work has shown that the cerebellum-like circuit in the dorsal cochlear nucleus performs the same function for the auditory system, canceling sound associated with the animal's own licking behavior (Singla et al., 2017). The cerebellum-like mechanosensory lateral line nucleus (MON) of fishes is possibly the most ancestral of these structures and may have been the starting point of cerebellar evolution (Hibi et al., 2017; Machold and Fishell, 2005; Montgomery et al., 2012; Murakami et al., 2005; Pose-Méndez et al., 2016; Sugahara et al., 2017; Wang et al., 2005). The results we report here support a role for the MON in predictive cancellation of reafference consistent with, and dependent on, the characteristic cerebellum-like circuitry shared with electrosensory and auditory systems.

We found that MON output cells (AENs) decreased their response to a mechanosensory stimulus that was time locked to respiratory and fin movement signals, while lateral line afferents projecting to the MON continued to convey their sensory response. Although complete cancellation was not observed in these experiments (even after 45 min of pairing in a few cases), AENs responded with a negative image of the mechanosensory response once the previously paired stimulus was withheld. This generation of a negative image to predictable sensory stimuli is the critical signature for the adaptive filter mechanism, which cancels that sensory input (Sawtell, 2017). Across the population, AENs generated negative images of sensory-evoked responses that were time locked to movement-related signals, while afferents did not. Poststimulus AEN activity was not affected by the same mechanosensory stimulus if it was presented uncoupled from movement-related signals. We did not investigate why or how receptive fields of different AENs were better driven by one or the other of these two stimulus variants. In future studies, this could be interesting to unpack, as it might indicate functional subclasses in the AEN population.

Although the effects reported here are statistically significant, it is of course difficult to know what 'effect sizes' would be functionally relevant in the MON circuit. Various circuit and cellular factors may constrain the amount of cancellation each individual AEN is able to achieve as well as its temporal precision. However, circuit-level mechanisms (such as synaptic pooling) may improve the ability of the ascending lateral line system to more effectively cancel the effects of reafference than any one individual cell in that system. In the future, it will be important to interrogate specific physiological constraints in this system (such as the specific spike timing-dependent plasticity rules at the parallel fiber synapse). In combination with computational modeling techniques, this would lead to a better understanding of the theoretical constraints imposed on the cancellation in individual neurons and potential hypotheses about circuit mechanisms that could overcome such constraints.

The effect sizes measured in this study may also be skewed by AENs that do not generate negative images, though there did not appear to be a bimodal split in effects among the population of AENs examined here (Figs 4A,C and 5C). From past studies we know that generally only 55–65% of electrosensory AENs in the dorsal nucleus in skates appear to exhibit the ability to generate negative images to predictable sensory input (Zhang and Bodznick, 2008). Anatomically, in the MON, two distinct populations of AENs can be identified, one of which forms a deeper layer called 'cell plate X', and both populations were likely included in this study (Schmidt and Bodznick, 1987). It will be interesting in future work to identify whether AENs from these two populations differ systematically in their ability to generate negative images.

The cancellation signal is the phenomenon that underlies the generation of a negative image to the induced stimulus pattern at stimulus offset. Although the development of a negative image to sensory responses implies the formation of a cancellation signal in the AEN, it cannot be directly measured with extracellular techniques. Future work aimed at studying this cancellation signal directly will require intracellular recordings. Additionally, future work implementing intracellular measurements and manipulation of individual AEN membrane potentials would enable direct comparisons between the mechanisms of synaptic plasticity in the MON and those established in other cerebellum-like structures.

The elegance of the cerebellum-like circuit is that a small set of biophysical rules generates a high-level function that enables organisms to more efficiently interact with their environment. The cerebellum-like circuit can be described as an adaptive filter (Dean and Porrill, 2011; Fujita, 1982; Montgomery and Bodznick, 1994). And the computation performed by the cerebellum-like circuit is well suited to any function in which an adaptive filter is appropriate. In the electrosensory, auditory and (as demonstrated by the results presented here) mechanosensory systems, the adaptive filter in the first-order cerebellum-like sensory structures learns a forward model that is the negative image of any sensory input predicted by granule cell responses (the filter's basis set), which includes signals related to the animal's own behavior. Functionally, the adaptive filter would enhance sensory processing in these sensory systems by eliminating reafference while maintaining sensitivity to externally generated sensory signals, which has been demonstrated in the mormyrid electrosensory lobe (Enikolopov et al., 2018). Critically, the specific function of a cerebellum-like circuit will depend on its inputs and outputs. Theoretical studies have described how an adaptive filter can form the basis for, *inter alia*, forward models, which have been useful in developing hypotheses about the role of the cerebellum proper in the context of a wide range of behavior (Ebner and Pasalar, 2008; Machado et al., 2015; Wolpert and Ghahramani, 2000). Ultimately, understanding cerebellar contributions to a remarkable diversity of behavior may best be understood from an evolutionary perspective (Montgomery and Bodznick, 2016; Perks and Montgomery, 2019).

Comparisons between the anatomy/physiology of the MON and the cerebellum can facilitate hypotheses about how the functionality of the cerebellum developed from its phylogenetic precursors (of which the MON is likely the most ancestral form) (Montgomery et al., 2012). The key feature that endows all cerebellum-like structures with their adaptive filter capability is plasticity at the synapses between the apical dendritic arbor of the output cells and the parallel fiber system.

One key difference between the MON and the mammalian cerebellum is that output cells of MON (AENs) are excitatory, while those of the mammalian cerebellum (Purkinje cells) are inhibitory. Output cells (eurodendroid cells) of the teleost cerebellum are excitatory, but this structure also contains inhibitory interneurons (named medium ganglion cells) that have elaborate dendritic arbors contacted by plastic parallel fiber synapses in the molecular layer (Han and Bell, 2003). Interestingly, excitatory output cells of the deep nuclei in the mammalian cerebellum are contacted by a plastic synapse originating from the same mossy fiber inputs that innervate granule cells providing parallel fibers to the cerebellar cortex (Gao et al., 2012; Mauk et al., 2014). It remains an open question what functional differences these anatomical differences provide to the systems in which they occur. Variation among cerebellum-like structures and the cerebellum in the composition and size of their granular cell domains likely underlies functional differences in their performance and implementation (Bratby et al., 2017a,b; Kennedy et al., 2014). Continued comparative studies among these structures will likely help unpack the impact that such differences have on the operation of the cerebellum-like circuit in different systems, including the cerebellum itself.

Studies on cerebellar origins and on the functions of cerebellum-like circuits highlight its sustained importance throughout vertebrate evolution. Yet, the function of the cerebellum remains hotly debated. Together, the results presented here provide strong support for the model of a conserved computation implemented by cerebellum-like circuits across vertebrates. Continued examination of: (1) diversity among cerebellum-like structures, (2) their evolutionary relationship and (3) differences among the sensory systems they serve scaffolds an evolutionary perspective on understanding how this conserved computation enables such diverse functions of the cerebellum in vertebrate neuroethology.

Acknowledgements
Data collected by K.E.P. were previously presented in thesis format (Perks, 2007). We would like to thank Billy Klem, Danny Sullivan and Eddie Enos at the Marine Biological Laboratory and the crew of the Environmental Lab at the Dominion Nuclear Plant in CT for collecting skates. We would like to thank Dr John Montgomery for his continued feedback.

Competing interests
The authors declare no competing or financial interests.

Author contributions
Conceptualization: K.E.P., A.K., D.B.; Methodology: K.E.P., A.K., D.B.; Software: K.E.P., D.B.; Validation: K.E.P., A.K., D.B.; Formal analysis: K.E.P.; Investigation: K.E.P., A.K.; Resources: D.B.; Data curation: K.E.P.; Writing - original draft: K.E.P.; Writing - review & editing: K.E.P., A.K., D.B.; Visualization: K.E.P.; Supervision: D.B.; Project administration: D.B.; Funding acquisition: D.B., K.E.P., A.K.

Funding
This work was supported by National Science Foundation (NSF) and Wesleyan University grants to D.B. Funding for K.E.P. while performing these experiments came in part from a grant from the HHMI Hughes V award for undergraduate education to Wesleyan University (52005211) in the form of a summer research fellowship. A.K. was supported in part by an NSF-REU Award (1659604) and a Wesleyan University Summer Research Fellowship. K.E.P. is currently supported through funding from the Simons Society of Fellows as a Junior Fellow.

Data availability
All data and analysis code (in open source Python format) pertaining to this study are available via the web-based repository G-Node: doi:10.12751/g-node.879051

References
Ayali, A., Gelman, S., Tytell, E. D. and Cohen, A. H. (2009). Lateral-line activity during undulatory body motions suggests a feedback link in closed-loop control of sea lamprey swimming. *Can. J. Zool.* **87**, 671-683. doi:10.1139/Z09-050

Bastian, J. (1995). Pyramidal-cell plasticity in weakly electric fish: a mechanism for attenuating responses to reafferent electrosensory inputs. *J. Comp. Physiol.* **176**, 63-78. doi:10.1007/BF00197753

Bastian, J. (1996). Plasticity in an electrosensory system. I. General features of a dynamic sensory filter. *J. Neurophysiol.* **76**, 2483-2496. doi:10.1152/jn.1996.76.4.2483

Bell, C. C. (2002). Evolution of cerebellum-like structures. *Brain Behav. Evol.* **59**, 312-326. doi:10.1159/000063567

Bell, C. C. and Grant, K. (1989). Corollary discharge inhibition and preservation of temporal information in a sensory nucleus of mormyrid electric fish. *J. Neurosci.* **9**, 1029-1044. doi:10.1523/JNEUROSCI.09-03-01029.1989

Bell, C., Bodznick, D., Montgomery, J. and Bastian, J. (1997a). The generation and subtraction of sensory expectations within cerebellum-like structures. *Brain Behav. Evol.* **50**, 17-31. doi:10.1159/000113352

Bell, C. C., Han, V. Z., Sugawara, Y. and Grant, K. (1997b). Synaptic plasticity in a cerebellum-like structure depends on temporal order. *Nature* **387**, 278-281. doi:10.1038/387278a0

Bell, C. C., Caputi, A. and Grant, K. (1997c). Physiology and plasticity of morphologically identified cells in the mormyrid electrosensory lobe. *J. Neurosci.* **17**, 6409-6423. doi:10.1523/JNEUROSCI.17-16-06409.1997

Bell, C. C., Caputi, A., Grant, K. and Serrier, J. (1993). Storage of a sensory pattern by anti-Hebbian synaptic plasticity in an electric fish. *Proc. Natl. Acad. Sci. USA* **90**, 4650-4654. doi:10.1073/pnas.90.10.4650

Bell, C. C., Finger, T. E. and Russell, C. J. (1981). Central connections of the posterior lateral line lobe in mormyrid fish. *Exp. Brain Res.* **42**, 9-22. doi:10.1007/BF00235724

Bell, C. C., Han, V. and Sawtell, N. B. (2008). Cerebellum-like structures and their implications for cerebellar function. *Annu. Rev. Neurosci.* **31**, 1-24. doi:10.1146/annurev.neuro.30.051606.094225

Bertetto, L. (2007). Functional synaptic plasticity in the electrosensory system of the little skate, *Raja erinacea*. *PhD dissertation*. Wesleyan University, Middletown, CT, USA.

Bodznick, D. (1989). Comparisons between electrosensory and mechanosensory lateral line systems. In *The Mechanosensory Lateral Line* (ed. S. Coombs, P. Gorner and H. Munz), pp. 653-678. New York, NY: Springer.

Bodznick, D. and Northcutt, R. G. (1980). Segregation of electro- and mechanoreceptive inputs to the elasmobranch medulla. *Brain Res.* **195**, 313-321. doi:10.1016/0006-8993(80)90067-0

Bodznick, D. and Schmidt, A. W. (1984). Somatotopy within the medullary electrosensory nucleus of the little skate, Raja erinacea. *J. Comp. Neurol.* **225**, 581-590. doi:10.1002/cne.902250408

Bodznick, D., Montgomery, J. C. and Carey, M. (1999). Adaptive mechanisms in the elasmobranch hindbrain. *J. Exp. Biol.* **202**, 1357-1364.

Boord, R. L. and Northcutt, R. G. (1982). Ascending lateral line pathways to the midbrain of the clearnose skate, Raja eglanteria. *J. Comp. Neurol.* **207**, 274-282. doi:10.1002/cne.902070307

Bratby, P., Sneyd, J. and Montgomery, J. (2017a). Computational architecture of the granular layer of cerebellum-like structures. *Cerebellum* **16**, 15-25. doi:10.1007/s12311-016-0759-z

Bratby, P., Sneyd, J. and Montgomery, J. (2017b). Sequential pattern formation in the cerebellar granular layer. *Cerebellum* **16**, 438-449. doi:10.1007/s12311-016-0820-y

Bullock, T. H., Bodznick, D. A. and Northcutt, R. G. (1983). The phylogenetic distribution of electroreception: evidence for convergent evolution of a primitive vertebrate sense modality. *Brain Res.* **287**, 25-46. doi:10.1016/0165-0173(83)90003-6

Dean, P. and Porrill, J. (2011). Evaluating the adaptive-filter model of the cerebellum. *J. Physiol.* **589**, 3459-3470. doi:10.1113/jphysiol.2010.201574

Duman, C. H. and Bodznick, D. (1996). A role for GABAergic inhibition in electrosensory processing and common mode rejection in the dorsal nucleus of the little skate, *Raja erinacea*. *J. Comp. Physiol. A* **179**, 797-807. doi:10.1007/BF00207358

Ebner, T. J. and Pasalar, S. (2008). Cerebellum predicts the future motor state. *Cerebellum* **7**, 583-588. doi:10.1007/s12311-008-0059-3

Enikolopov, A. G., Abbott, L. F. and Sawtell, N. B. (2018). Internally generated predictions enhance neural and behavioral detection of sensory stimuli in an electric fish. *Neuron* **99**, 135-146.e133. doi:10.1016/j.neuron.2018.06.006

Finger, T. E., Bell, C. C. and Carr, C. (1986). Comparisons among electroreceptive teleosts: why are the electrosensory systems so similar? In *Electroreception* (ed. T. H. Bullock and W. Heiligenberg), pp. 465-481. New York: John Wiley & Sons, Inc.

Fujita, M. (1982). Adaptive filter model of the cerebellum. *Biol. Cybern.* **45**, 195-206. doi:10.1007/BF00336192

Gao, Z., van Beugen, B. J. and De Zeeuw, C. I. (2012). Distributed synergistic plasticity and cerebellar learning. *Nat. Rev. Neurosci.* **13**, 619-635. doi:10.1038/nrn3312

Han, V. Z. and Bell, C. C. (2003). Physiology of cells in the central lobes of the mormyrid cerebellum. *J. Neurosci.* **23**, 11147-11157. doi:10.1523/JNEUROSCI.23-35-11147.2003

Harvey-Girard, E., Lewis, J. and Maler, L. (2010). Burst-induced anti-Hebbian depression acts through short-term synaptic dynamics to cancel redundant sensory signals. *J. Neurosci.* **30**, 6152-6169. doi:10.1523/JNEUROSCI.0303-10.2010

Hibi, M., Matsuda, K., Takeuchi, M., Shimizu, T. and Murakami, Y. (2017). Evolutionary mechanisms that generate morphology and neural-circuit diversity of the cerebellum. *Dev. Growth Differ.* **59**, 228-243. doi:10.1111/dgd.12349

Hjelmstad, G., Parks, G. and Bodznick, D. (1996). Motor corollary discharge activity and sensory responses related to ventilation in the skate vestibulolateral cerebellum: implications for electrosensory processing. *J. Exp. Biol.* **199**, 673-681.

Kennedy, A., Wayne, G., Kaifosh, P., Alvina, K., Abbott, L. F. and Sawtell, N. B. (2014). A temporal basis for predicting the sensory consequences of motor commands in an electric fish. *Nat. Neurosci.* **17**, 416-422. doi:10.1038/nn.3650

Kim, A. J., Fitzgerald, J. K. and Maimon, G. (2015). Cellular evidence for efference copy in Drosophila visuomotor processing. *Nat. Neurosci.* **18**, 1247-1255. doi:10.1038/nn.4083

Kim, A. J., Fenk, L. M., Lyu, C. and Maimon, G. (2017). Quantitative predictions orchestrate visual signaling in Drosophila. *Cell* **168**, 280-294.e212. doi:10.1016/j.cell.2016.12.005

Machado, A. S., Darmohray, D. M., Fayad, J., Marques, H. G. and Carey, M. R. (2015). A quantitative framework for whole-body coordination reveals specific deficits in freely walking ataxic mice. *eLife* **4**, e07892. doi:10.7554/eLife.07892

Machold, R. and Fishell, G. (2005). Math1 is expressed in temporally discrete pools of cerebellar rhombic-lip neural progenitors. *Neuron* **48**, 17-24. doi:10.1016/j.neuron.2005.08.028

Mauk, M. D., Li, W., Khilkevich, A. and Halverson, H. (2014). Cerebellar mechanisms of learning and plasticity revealed by delay eyelid conditioning. *Int. Rev. Neurobiol.* **117**, 21-37. doi:10.1016/B978-0-12-420247-4.00002-6

Mensinger, A. F., Van Wert, J. C. and Rogers, L. S. (2018). Lateral line sensitivity in free-swimming toadfish *Opsanus tau*. *J. Exp. Biol.* **222**, jeb190587. doi:10.1242/jeb.190587

Montgomery, J. and Bodznick, D. (2016). *Evolution of the Cerebellar Sense of Self*. Oxford University Press.

Montgomery, J. C. and Bodznick, D. (1994). An adaptive filter that cancels self-induced noise in the electrosensory and lateral line mechanosensory systems of fish. *Neurosci. Lett.* **174**, 145-148. doi:10.1016/0304-3940(94)90007-8

Montgomery, J. C., Bodznick, D. and Halstead, M. B. D. (1996). Hindbrain signal processing in the lateral line system of the dwarf scorpionfish Scopeana papillosus. *J. Exp. Biol.* **199**, 893-899.

Montgomery, J. C., Bodznick, D. and Yopak, K. E. (2012). The cerebellum and cerebellum-like structures of cartilaginous fishes. *Brain Behav. Evol.* **80**, 152-165. doi:10.1159/000339868

Muller, S. Z., Zadina, A. N., Abbott, L. F. and Sawtell, N. B. (2019). Continual learning in a multi-layer network of an electric fish. *Cell* **179**, 1382-1392.e10. doi:10.1016/j.cell.2019.10.020

Murakami, Y., Uchida, K., Rijli, F. M. and Kuratani, S. (2005). Evolution of the brain developmental plan: Insights from agnathans. *Dev. Biol.* **280**, 249-259. doi:10.1016/j.ydbio.2005.02.008

Nelson, M. E. and Paulin, M. G. (1995). Neural simulations of adaptive reafference suppression in the elasmobranch electrosensory system. *J. Comp. Physiol. A* **177**, 723-736. doi:10.1007/BF00187631

New, J. G., Coombs, S., McCormick, C. A. and Oshel, P. E. (1996). Cytoarchitecture of the medial octavolateralis nucleus in the goldfish, Carassius auratus. *J. Comp. Neurol.* **366**, 534-546. doi:10.1002/(SICI)1096-9861(19960311)366:3<534::AID-CNE11>3.0.CO;2-P

Oertel, D. and Young, E. D. (2004). What's a cerebellar circuit doing in the auditory system? *Trends Neurosci.* **27**, 104-110. doi:10.1016/j.tins.2003.12.001

Palmer, L. M., Deffenbaugh, M. and Mensinger, A. F. (2005). Sensitivity of the anterior lateral line to natural stimuli in the oyster toadfish, *Opsanus tau*, (Linnaeus). *J. Exp. Biol.* **208**, 3441-3450. doi:10.1242/jeb.01766

Perks, K. E. and Montgomery, J. C. (2019). Understanding cerebellum in vertebrate neuroethology: from sensing in sharks and electric fish to motor sequences in movement and bird song. *Behav. Neurosci.* **133**, 267-281. doi:10.1037/bne0000317

Perks, K. E. (2007). Adaptive sensory filtering in the cerebellar-like mechanosensory nucleus of the hindbrain in raja erinacea. *Masters Thesis*. Wesleyan University, Middletown, CT, USA. Retrieved from wesscholar.wesleyan.edu/etd_mas_theses/6/.

Pose-Méndez, S., Candal, E., Mazan, S. and Rodríguez-Moldes, I. (2016). Morphogenesis of the cerebellum and cerebellum-related structures in the shark Scyliorhinus canicula: insights on the ground pattern of the cerebellar ontogeny. *Brain Struct. Funct.* **221**, 1691-1717. doi:10.1007/s00429-015-0998-7

Poulet, J. F. and Hedwig, B. (2003). Corollary discharge inhibition of ascending auditory neurons in the stridulating cricket. *J. Neurosci.* **23**, 4717-4725. doi:10.1523/JNEUROSCI.23-11-04717.2003

Requarth, T. and Sawtell, N. B. (2014). Plastic corollary discharge predicts sensory consequences of movements in a cerebellum-like circuit. *Neuron* **82**, 896-907. doi:10.1016/j.neuron.2014.03.025

Roberts, P. D. and Bell, C. C. (2000). Computational consequences of temporally asymmetric learning rules: II. Sensory image cancellation. *J. Comput. Neurosci.* **9**, 67-83. doi:10.1023/A:1008938428112

Roberts, B. L. and Russell, I. J. (1972). The activity of lateral-line efferent neurones in stationary and swimming dogfish. *J. Exp. Biol.* **57**, 435-448.

Russell, I. J. (1971). The role of the lateral-line efferent system in Xenopus laevis. *J. Exp. Biol.* **54**, 621-641.

Russell, I. J. and Roberts, B. L. (1974). Active reduction of lateral line sensitivity in swimming dogfish. *J. Comp. Physiol.* **94**, 7-15. doi:10.1007/BF00610153

Sawtell, N. B. (2017). Neural mechanisms for predicting the sensory consequences of behavior: insights from electrosensory systems. *Annu. Rev. Physiol.* **79**, 381-399. doi:10.1146/annurev-physiol-021115-105003

Schmidt, A. W. and Bodznick, D. (1987). Afferent and efferent connections of the vestibulolateral cerebellum of the little skate, Raja erinacea. *Brain Behav. Evol.* **30**, 282-302. doi:10.1159/000118652

Shimazaki, H. and Shinomoto, S. (2010). Kernel bandwidth optimization in spike rate estimation. *J. Comp. Neuro* **29**, 171-182. doi:10.1007/s10827-009-0180-4

Singla, S., Dempsey, C., Warren, R., Enikolopov, A. G. and Sawtell, N. B. (2017). A cerebellum-like circuit in the auditory system cancels responses to self-generated sounds. *Nat. Neurosci.* **20**, 943-950. doi:10.1038/nn.4567

Sugahara, F., Murakami, Y., Pascual-Anaya, J. and Kuratani, S. (2017). Reconstructing the ancestral vertebrate brain. *Dev. Growth Differ.* **59**, 163-174. doi:10.1111/dgd.12347

Suriano, C. M. and Bodznick, D. (2018). Evidence for generative homology of cerebellum and cerebellum-like structures in an elasmobranch fish based on Pax6, Cbln1 and Grid2 expression. *J. Comp. Neurol.* **526**, 2187-2203. doi:10.1002/cne.24473

Wang, V. Y., Rose, M. F. and Zoghbi, H. Y. (2005). Math1 expression redefines the rhombic lip derivatives and reveals novel lineages within the brainstem and cerebellum. *Neuron* **48**, 31-43. doi:10.1016/j.neuron.2005.08.024

Wolpert, D. M. and Ghahramani, Z. (2000). Computational principles of movement neuroscience. *Nat. Neurosci.* **3** Suppl, 1212-1217. doi:10.1038/81497

Yger, P., Spampinato, G. L. B., Esposito, E., Lefebvre, B., Deny, S., Gardella, C., Stimberg, M., Jetter, F., Zeck, G. Picaud, S. et al. (2018). A spike sorting toolbox for up to thousands of electrodes validated with ground truth recordings in vitro and in vivo. *eLife* **7**:e34518. doi:10.7554/eLife.34518

Zhang, Z. and Bodznick, D. (2008). Plasticity in a cerebellar-like structure: suppressing reafference during episodic behaviors. *J. Exp. Biol.* **211**, 3720-3728. doi:10.1242/jeb.020099

Zhang, Z. and Bodznick, D. (2010). The importance of N-methyl-D-aspartate (NMDA) receptors in subtraction of electrosensory reafference in the dorsal nucleus of skates. *J. Exp. Biol.* **213**, 2700-2709. doi:10.1242/jeb.041186